

Distinct Single-Cell Morphological Dynamics under Beta-Lactam Antibiotics

Zhizhong Yao,^{1,3} Daniel Kahne,^{1,4,*} and Roy Kishony^{2,3,*}¹Department of Chemistry and Chemical Biology²School of Engineering and Applied Sciences

Harvard University, 12 Oxford Street, Cambridge, MA 02138, USA

³Department of Systems Biology⁴Department of Biological Chemistry and Molecular Pharmacology

Harvard Medical School, 200 Longwood Avenue, Boston, MA 02115, USA

*Correspondence: kahne@chemistry.harvard.edu (D.K.), roy_kishony@hms.harvard.edu (R.K.)

<http://dx.doi.org/10.1016/j.molcel.2012.09.016>

SUMMARY

The bacterial cell wall is conserved in prokaryotes, stabilizing cells against osmotic stress. Beta-lactams inhibit cell-wall synthesis and induce lysis through a bulge-mediated mechanism; however, little is known about the formation dynamics and stability of these bulges. To capture processes of different timescales, we developed an imaging platform combining automated image analysis with live-cell microscopy at high time resolution. Beta-lactam killing of *Escherichia coli* cells proceeded through four stages: elongation, bulge formation, bulge stagnation, and lysis. Both the cell wall and outer membrane (OM) affect the observed dynamics; damaging the cell wall with different beta-lactams and compromising OM integrity cause different modes and rates of lysis. Our results show that the bulge-formation dynamics are determined by how the cell wall is perturbed. The OM plays an independent role in stabilizing the bulge once it is formed. The stabilized bulge delays lysis and allows recovery upon drug removal.

INTRODUCTION

Beta-lactam antibiotics have been widely used in the clinic for more than half a century and account for the largest share in the worldwide antibiotic market (Hamad, 2010). The cellular target of beta-lactams is the peptidoglycan (PG). This thin layer of biopolymer mesh, which serves to maintain cell morphology and balance turgor pressure, is composed of long glycan chains and peptide crosslinks (Höltje, 1998). Peptide crosslinks are formed by the transpeptidase activity of penicillin-binding proteins (PBPs). Beta-lactam antibiotics covalently bind to PBPs and inhibit crosslink formation, the last stage of PG synthesis (Tipper and Strominger, 1965; Wise and Park, 1965). Inhibition of PG synthesis by beta-lactams has various effects on cell shape due to their ability to bind to one or more PBPs involved

in cell division, elongation, and shape maintenance (Spratt, 1975). It has been proposed that inhibition of crosslink formation by beta-lactams combined with misregulated cell-wall degradation by PG hydrolases results in the accumulation of PG defects, which ultimately leads to cell lysis (Chung et al., 2009).

The physical process of PG defect formation and subsequent lysis is poorly understood. Previous literature suggested a bulge-mediated process (Chung et al., 2009; Huang et al., 2008), and the reported rates of lysis have been loosely characterized as slow and fast (de Pedro et al., 2002). However, in the absence of systematic characterization of bulge-formation dynamics and their variability across individual cells, it is unclear whether lysis occurs uniformly within isogenic cell populations, or whether distinct physical processes act in different cells. Furthermore, it is unknown whether different beta-lactam antibiotics cause similar or distinct modes of lysis.

In addition to the PG layer, the cell envelope also includes inner and outer membranes (IM and OM), both of which are essential for cell viability. Unlike the IM, which is a simple phospholipid bilayer, the OM is asymmetric (Funahara and Nikaido, 1980; Kamio and Nikaido, 1976). Its outer-leaflet lipopolysaccharide (LPS) layer serves as a protective barrier against detergents and hydrophobic antibiotics (e.g., vancomycin), with embedded porins that allow diffusion of small hydrophilic molecules including nutrients and beta-lactams (Pagès et al., 2008). An LPS molecule consists of lipid A, LPS core, and the O antigen. Absence of O antigen makes Gram-negative bacteria hypersensitive toward hydrophobic antibiotics, detergents, and host proteins (Silhavy et al., 2010). Although PG is covalently attached to the OM, and recent studies have shown that OM lipoproteins regulate PG synthesis (Paradis-Bleau et al., 2010; Typas et al., 2010), the potential role of the OM in beta-lactam-induced cell lysis has not been studied.

In order to study bulge formation and lysis in greater detail, we developed a live-cell imaging platform to monitor the morphological dynamics of *E. coli* cells under beta-lactam treatment at high time resolution. This platform allows a high-throughput study of single-cell shape dynamics over long periods of time, at a time resolution that captures the fast lysis dynamics (~2 hr, at ~8 frames/s). We used this platform to characterize variability in bulge formation and lysis within

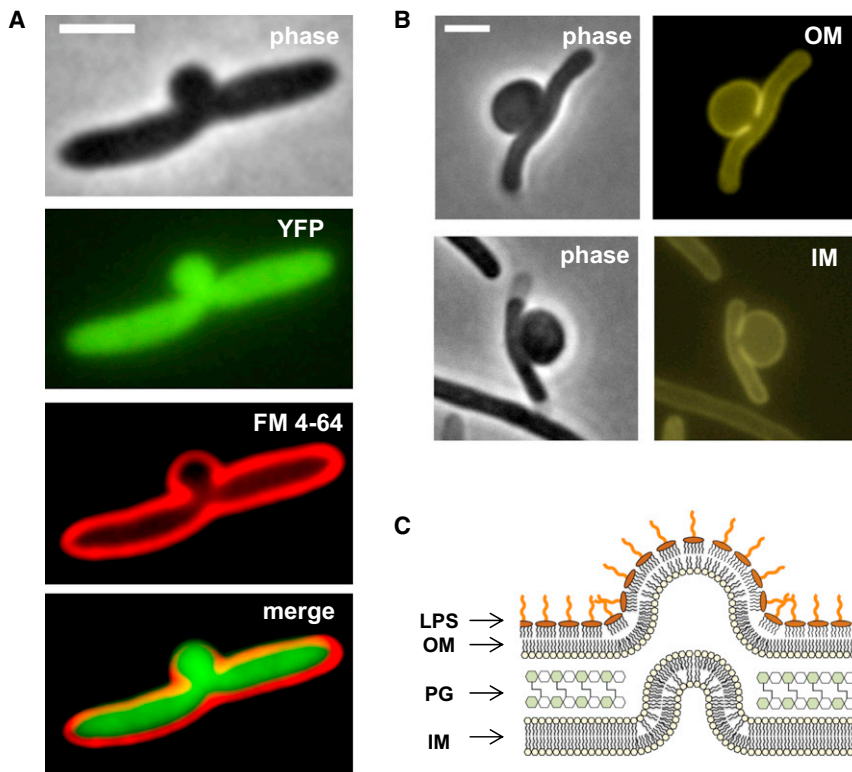


Figure 1. Both Inner and Outer Membranes Are Intact in Bulging Cells

(A and B) Phase-contrast and fluorescence images of bulging cells under cephalaxin treatment (A, cytoplasmic YFP and FM4-64 membrane staining; B, ZipA-mCherry, IM marker, and ⁵⁹Pal-mCherry, OM marker). Membrane protrusions indicate PG defects at the potential division site. Leakage of cytoplasmic YFP into the bulge suggests redistribution of cytosolic materials from the cell filament to the midcell bulge.

(C) Schematic illustration of a bulge as a cell-wall-less cytosolic protrusion surrounded by both the IM and the OM. LPS is exclusively located at the outer leaflet of the OM, and its long glycan chains facilitate a micelle-like close-packed structure.

All scale bars represent 2 μm . See also Figure S1.

isogenic cells under different beta-lactams. We chose to primarily focus on cephalaxin (Keflex), because it targets PBP3 (FtsI), the only essential PBP involved in cell division, which is the best-understood pathway for PG biogenesis (Chung et al., 2009). We also tested cefsulodin, which targets elongation-specific PBP1a and PBP1b, and ampicillin, which broadly targets all PBPs. Finally, we applied genetic and chemical perturbations to test the possible role of OM in beta-lactam killing.

RESULTS

Beta-Lactam-Induced Bulges Are Enclosed by Both IM and OM

To understand the physical processes behind bulge formation, we determined the structural components of the bulge. First, we asked whether beta-lactam-induced bulges contain the same materials as cytoplasm. We used an *E. coli* strain expressing cytoplasmic yellow fluorescent protein (YFP) and examined the morphology of these cells grown in liquid culture under cephalaxin treatment. YFP and membrane stain images suggested that cytosol materials leak through PG defects and deform the double membranes at the midcell site (Figure 1A). Next, to examine whether both membranes are intact, we used two additional *E. coli* strains with mCherry fused to an IM protein and an OM protein (Paradis-Bleau et al., 2010). Fluorescence images showed that both IM and OM remain intact in bulging cells (Figure 1B; Figure S1 available online). We concluded that bulges are protrusions of cytoplasmic materials surrounded by both IM and OM (Figure 1C).

Four Distinct Physical Phases Leading to Cell Lysis

Beta-lactam-induced cell lysis requires disintegration of all three layers of the cell envelope, which involves processes that take place at a range of timescales. In order to characterize each of these processes, it is necessary to acquire time-lapse movies with adaptive time resolutions in accordance with different

stages leading to cell lysis (Experimental Procedures). The resulting time resolution of our imaging platform varies from ~ 125 ms/frame to ~ 12.5 s/frame for fast and slow processes, respectively. Quantitative image analysis allows continuous measurement of cell length and bulge depth throughout beta-lactam treatment (Figure 2A and Movie S1).

A typical progression to cell lysis observed by time-lapse microscopy of cells under cephalaxin involves four distinct physical phases: filamentation, bulge formation, bulge stagnation, and lysis (membrane rupture). Following exposure to the drug ($t_0 = 0$), we observed a long period of cell elongation (Figure 2B, ~ 70 min), during which cell length kept increasing at a normal rate without a change in cell width (Figure 2A, t_1 ; Figure 2B). Then, a bulge formed abruptly at the potential division site. We define the time between the beginning (t_2) and end (t_3) of bulge formation as bulge-formation time τ_B (Figure 2C, $\tau_B = t_3 - t_2 = \sim 150$ ms; higher time resolution in Figure S2). This second phase is marked by a large increase in bulge depth and simultaneous shrinkage of cell length, indicating that bulges form out of existing cytosol and membranes instead of newly synthesized materials. Some of the cells also underwent “cracking” during bulge formation, which we quantified by the change in the angle ($\Delta\theta$) measured at the bulging site. After its abrupt formation, the midcell bulge is typically stable for an intermediate time (\sim minutes) before final lysis. We define this delay between the onset of bulge formation (t_2) and final lysis (t_4) as bulge lifetime τ_{BL} (Figure 2C, $\tau_{BL} = t_4 - t_2 = \sim 3$ min). Finally, after a period of stagnation, we observed a fast increase in bulge depth followed by membrane rupture and lysis (t_5). Cells treated with ampicillin showed similar characteristics, with additional swelling at the midcell site (Figure S3).

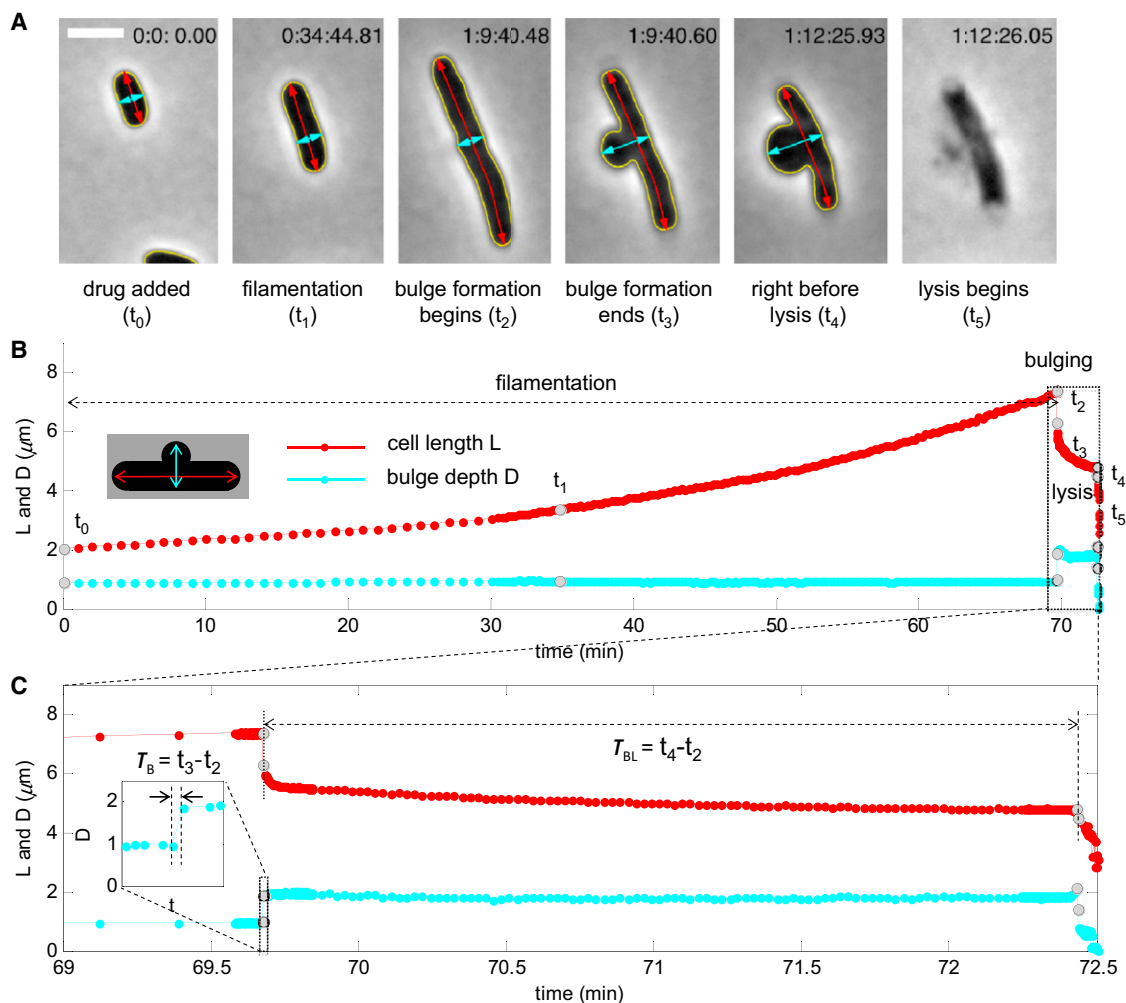


Figure 2. Live-Cell Microscopy with Automated Imaging Analysis Reveals Bulge Formation as an Intermediate Step toward Lysis

(A) Selected images of a representative *E. coli* cell at different stages of cephalixin treatment (yellow, cell contour; red, cell length; cyan, bulge depth). The time of these snapshots ($t_0 \sim t_5$) is indicated in gray dots in (B).

(B and C) Measurement of cell length (L) and bulge depth (D) of a representative *E. coli* cell throughout beta-lactam treatment (B) and during bulging and lysis (C, zoom-in view of the box in B). Both bulge-formation time (τ_B) and bulge lifetime (τ_{BL} , zoom-in inset in C) are defined based on bulge-depth measurements. Adaptive time resolutions were adopted to characterize processes with different kinetics: 1 min/frame for the first 30 min after adding drug, 12.5 s/frame for filamentation and bulge stagnation, and ~ 125 ms/frame for bulge formation and final lysis. Notice the simultaneous cell-length shrinkage during the abrupt bulge formation and the second increase in bulge depth right before lysis.

Scale bar represents 2 μm . See also Figure S2 and Movie S1.

To evaluate the generality of the observed progression for other beta-lactams, we carried out similar experiments for cefsulodin, a beta-lactam with a different profile from cephalixin and ampicillin. Cefsulodin targets PBP1a and PBP1b in *E. coli*, and it is generally considered to be elongation specific (Jacoby and Young, 1991). We first examined cells grown in liquid culture under cefsulodin treatment. Bulges still formed at the midcell site; however, YFP and membrane stain images of these cells did not show membrane gaps near the bulging site (Figure 3A). Selective images of a representative cell show that, unlike cephalixin and ampicillin, cefsulodin does not block septation; the representative cell underwent two rounds of division before lysis. Bulges formed at nascent poles on septated filaments, and lysis

occurred separately in daughter cells (Figure 3B; Movie S2). We conclude that there is a common pathway to cell lysis under all beta-lactams tested. However, morphological characteristics of each step vary for different classes of beta-lactams based on their specific cellular targets.

Three Modes of Bulge Formation within Isogenic Cell Populations

Do all *E. coli* cells follow the same morphological dynamics as shown in representative cells? To answer this question, we recorded and analyzed the morphological dynamics of ~ 200 wild-type cells under cephalixin treatment, focusing on bulge formation. We found that cells separated into three distinct

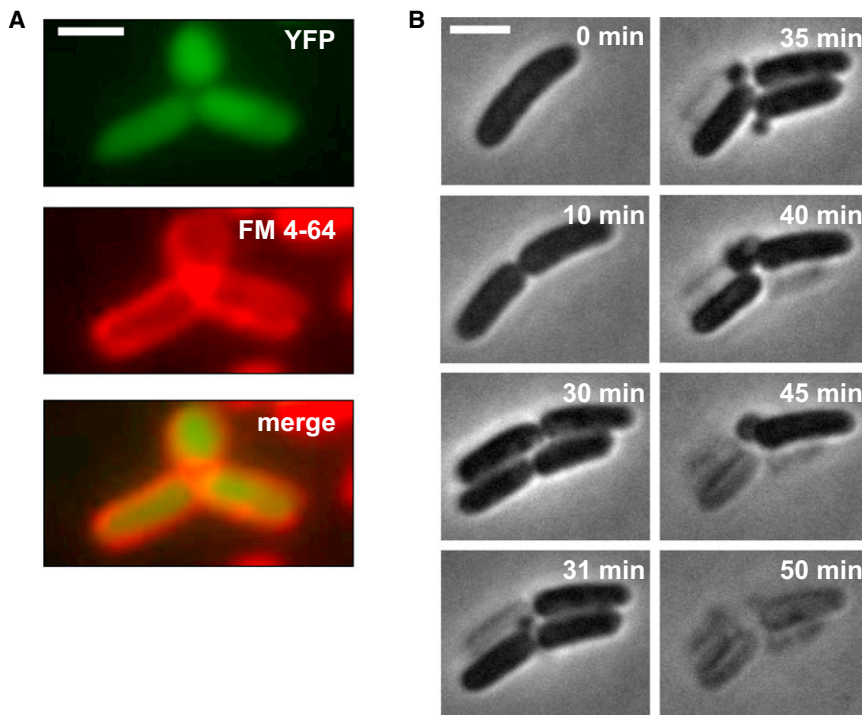


Figure 3. Cefsulodin-Induced Lysis Shows Shared as well as Distinct Features

(A) Fluorescence images of bulging cells treated with cefsulodin (cytoplasmic YFP and FM4-64 membrane staining). No obvious membrane gap was observed between the bulge and the filament. (B) Selected snapshots of a representative *E. coli* cell at different stages of cefsulodin treatment. Bulge formation and separate lysis events occur at nascent poles on septated filaments. Scale bar represents 2 μm . See also [Figure S3](#) and [Movie S2](#).

patterns on the basis of how fast the bulge is formed and its final morphology. Histogram plots of both bulge-formation time (τ_{BL}) and cracking angle ($\Delta\theta$) showed bimodal distribution ([Figure 4A](#)). Approximately half of the cells developed bulges abruptly, within less than 0.5 s ([Figure 4A](#), red dots; [Figure 4B](#)), whereas the rest of the population formed bulges gradually, over the course of several minutes ([Figure 4A](#), yellow and blue dots; [Figures 4C](#) and [4D](#)). Many of the fast-bulging cells completed bulge formation within ~ 150 ms, the time-resolution limit of our imaging platform. Additional measurements using a faster camera (~ 5 ms/frame) resolved the bulge-formation time of a representative fast-bulging cell to less than 100 ms ([Figure S2](#)). A small fraction of the slow-bulging cells displayed a cracking pattern, wherein filaments bent at the potential division site as bulges were slowly formed ([Figure 4D](#)). The typical cracking angle is $\sim 20^\circ$ ([Figure 4A](#), top panel). We hypothesized that the heterogeneity of bulge formation observed in isogenic cell populations might be due to different elongation states upon exposure to the drug. To test this hypothesis, we took initial cell length as a proxy for elongation states; however, no correlation was found between initial cell length and bulge-formation time ([Figure S4](#)). Moreover, these three distinct bulging patterns were also observed in cells treated with a different concentration of cephalixin and with ampicillin ([Figure S4](#)).

The Mode of Bulge Formation Affects Bulge Stability

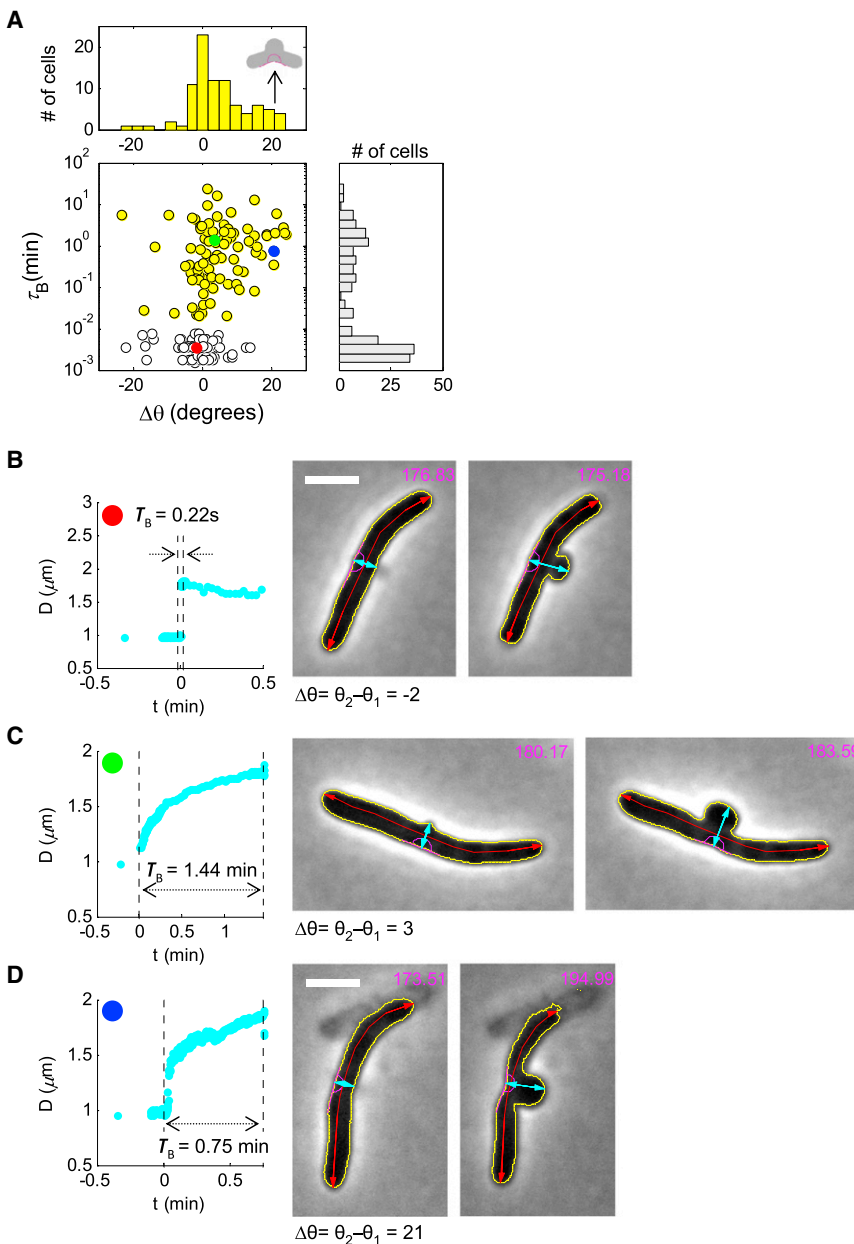
Do distinct modes of bulge formation affect bulge stability? To answer this question, we quantified the bulge lifetime of the same ~ 200 cephalixin-treated cells. Again we observed significant variability within isogenic cell populations. The distribution of bulge lifetime varied by almost three orders of magnitude ([Figure 5A](#)). This variability correlated with the rate of bulge forma-

tion; slow-bulging cells were much more stable ($\tau_{\text{BL}} > 10^0$ min) than fast-bulging cells ([Figure 5A](#)). To verify this correlation, we examined whether cells treated with cefsulodin, which showed a different mechanism of bulge formation, would also exhibit different bulge stability. The percentage of fast-lysing cells increased significantly under cefsulodin treatment ([Figure 5B](#)). Alternatively, variability in bulge stability could also arise from different bulge sizes in fast- and slow-bulging cells; however, measurements of change in cell length and bulge depth before and after bulge formation excluded such a possibility ([Figure S4](#)). We conclude that the mode of cell-wall damage, through its effect on the rate of bulge formation, can affect bulge stability and ultimately cell lysis.

Outer Membrane Integrity Affects Bulge Stability

While bulge stability correlates with the rate of bulge formation, not all of its large variability is explained. Because the OM encloses the bulge, we hypothesized that its strength may affect bulge stability and identified two ways to influence OM integrity. First, we used a chelating agent (EDTA) to remove Mg^{2+} , which stabilizes the electrostatic interactions among adjacent LPS molecules in the OM ([Nikaido and Vaara, 1985](#)). Second, we used an *E. coli* strain carrying an *lptD* mutation that compromises its efficiency in the assembly of LPS molecules at the OM ([Freinkman et al., 2011](#)). Whereas EDTA may have nonspecific effects on other cellular processes, the *lptD* mutation is specific to OM biogenesis. Indeed, the measurement of minimum inhibitory concentration for *lptD* mutants showed a 30-fold increase in susceptibility toward vancomycin, but it also showed unchanged susceptibility toward hydrophilic antibiotics, including cephalixin ([Figure S5](#)). Without additional stress, cells with a leaky OM increase in biomass at a normal rate with only mild defects in daughter-cell separation ([Figure S5](#)). These results confirmed that the *lptD* mutation compromises OM integrity without major effect on other aspects of cell growth.

We applied our imaging platform to monitor the progression to lysis of EDTA-treated wild-type cells and *lptD* mutants under cephalixin treatment. Both OM perturbations reduced bulge stability dramatically ([Figures 5C](#) and [5D](#)). For many fast-lysing cells ($\tau_{\text{BL}} < 10^{-2}$ min), bulge formation did not reach completion



in both scenarios and membranes ruptured prematurely (Figure S5). Unchanged susceptibility to cephalixin ruled out higher effective-drug concentration as the cause for reduced bulge lifetime in *lptD* mutants. Conversely, stabilizing the LPS layer by adding Mg^{2+} lengthened bulge lifetime and generated stable spheroplasts (Figure 6A and Movie S4) (Birdsell and Cotarobles, 1967; Joseleau-Petit et al., 2007; Lederberg and St Clair, 1958). Lysis still occurred when 0.3 M sucrose was used to generate similar osmolarity; therefore, the hypertonic environment alone cannot explain the protective effect of Mg^{2+} . These results suggested that, in Gram-negative bacteria, mechanical support provided by the LPS layer prevents the bulge from rupturing despite internal turgor pressure.

Figure 4. Three Distinct Bulging Patterns and Dynamics within Isogenic Cell Populations

(A–D) Scatter and histogram plots of bulge-formation time (τ_B) and cracking angle ($\Delta\theta$) reveal three different bulging patterns in response to cell-wall damage by cephalixin: fast bulging without cracking (B, red dot, $\tau_B < 10^{-2}$ min), slow bulging without cracking (C, green dot, $\tau_B > 10^{-2}$ min), and slow bulging with cracking (D, blue dot, $\tau_B > 10^{-2}$ min). Yellow dots and bar graphs represent slow-bulging cells (A, top and left panels). Gray bars represent all isogenic cells examined (A, right panel; $n = 195$).

(B–D) Representative bulge depth (D) measurement and snapshots of cells before (t_2) and after (t_3) bulge formation for each bulging pattern. Magenta lines represent measurement of cracking angles.

All scale bars represent 2 μm . See also Figure S4 and online supplemental movies for cell 6, cell 75, and cell 123.

Bulging Cells Resume Normal Growth upon Drug Removal

Is bulge formation a reversible process? Are bulging cells able to revert to rod shape upon drug removal? To answer these questions, we acquired time-lapse microscopy of bulging cells upon drug removal. Mg^{2+} was added throughout for prevention of lysis caused by washing, resuspension, and transfer onto our imaging platform (Experimental Procedures). After 2 hr, all bulging cells (20 out of 20) escaped lysis and formed rapidly growing microcolonies. Notably, such rapid recovery was initiated by pinching off poles of the rod-shaped filaments (Figure 6B and Movie S5). The bulge itself, which continued to grow, did not contribute to the reversion of new, healthy rod-shaped cells. Consistently, all spheroplasts examined (20 out of 20) never recovered upon drug removal and ultimately lysed. To summarize, bulging

cells, unlike spheroplasts, are in a metastable state, which can lead to either cell lysis or recovery upon drug removal (Figure 6C).

DISCUSSION

Using live-cell microscopy at high time resolution combined with automated image analysis, this study characterized the morphological dynamics of single cells under treatment with beta-lactam antibiotics. We found that cell lysis induced by beta-lactam antibiotics shares a common progression through four physical phases: elongation, bulge formation, bulge stagnation, and lysis. Two of these stages, bulge formation and bulge stagnation,

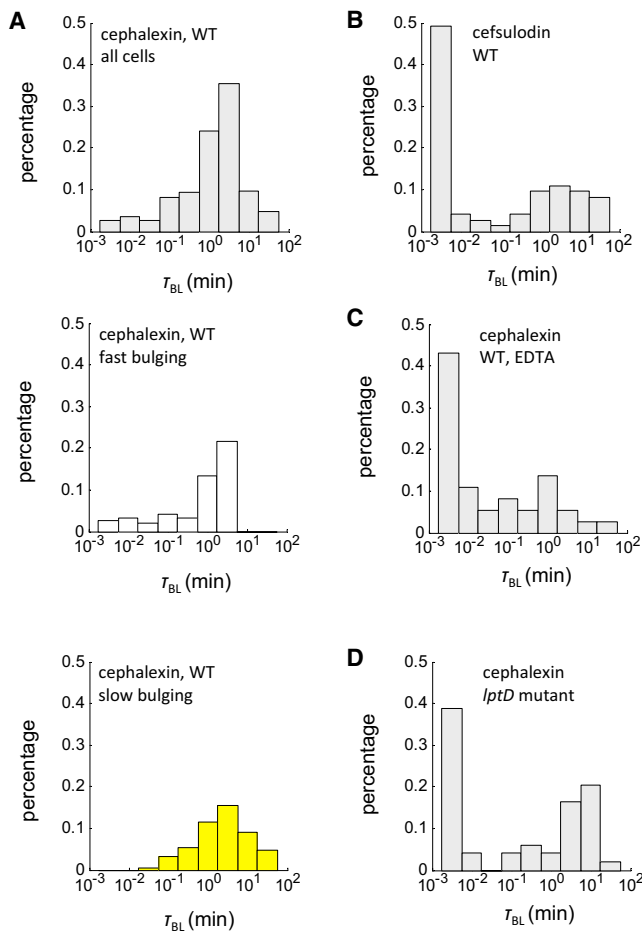


Figure 5. Both Modes of Bulge Formation and Integrity of the OM Affect Bulge Stability

(A) Bulge-lifetime distribution of all wild-type cells (WT, top panel, $n = 195$) and subpopulations of fast-bulging cells (middle panel, $n = 95$) and slow-bulging cells (bottom panel, $n = 100$) under cephalaxin treatment ($50 \mu\text{g/ml}$).

(B) Bulge-lifetime distribution of WT cells ($n = 73$) under cefsulodin treatment ($50 \mu\text{g/ml}$).

(C and D) Bulge-lifetime distribution of EDTA-treated cells (C, $n = 37$) and *lptD* mutants (D, $n = 49$) under cephalaxin treatment ($50 \mu\text{g/ml}$).

See also Figure S5 and Movie S3.

showed large variability within isogenic cell populations. Understanding the factors contributing to the variability in bulge stability could be critical, because cells with stabilized bulges demonstrated capacity to escape lysis upon drug removal.

We identified two factors that influence the stability of the bulge. First, genetic and chemical perturbations to the OM strongly affect the stability of the bulge. It is conceivable that isogenic cells can vary in the abundance and activity of cellular components that affect OM integrity, such as the LPS transport pathway or the Tol-Pal complex (Gerding et al., 2007). Second, the stability of the bulge is affected by the mode of bulge formation, with fast-formed bulges being less stable. Bulge formation is ultimately a cell-wall-dependent process; membrane eruption requires the formation of a cell-wall lesion exceeding a critical

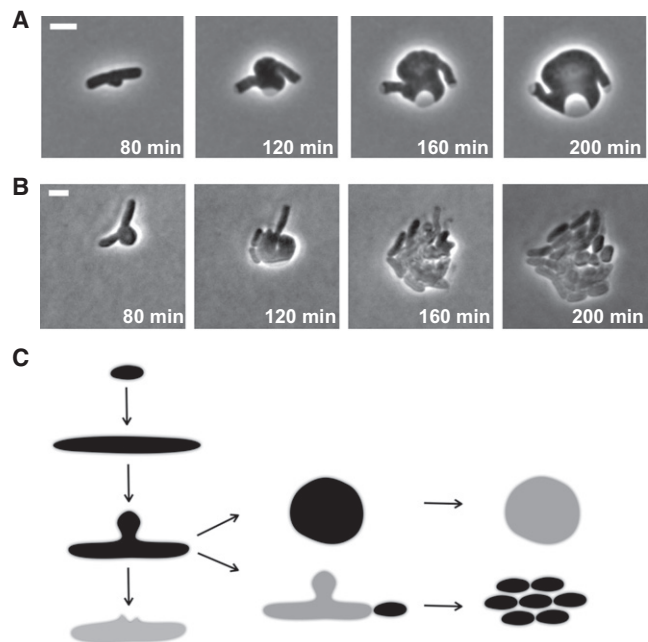


Figure 6. Alternative Cell Fates of Bulging Cells

(A) Snapshots of spheroplast formation induced by cephalaxin. Initial stages of spheroplast formation are identical with those of beta-lactam-induced cell lysis. These remarkably stable spheroplasts lysed immediately upon Mg^{2+} removal, as judged by the OD drop of the liquid culture.

(B) Snapshots of bulging cells reverting to rod-shaped cells upon drug removal. Cells with stabilized bulges escaped lysis by initiating septation near old poles and pinching off portions of the filaments.

(C) Proposed model of beta-lactam-induced bulges as a metastable state toward cell lysis, spheroplast formation, or reversion to rod-shaped cells.

All scale bars represent $2 \mu\text{m}$. See also Movies S4 and S5.

size (Daly et al., 2011). Indeed, we find that perturbing the cell wall with different classes of beta-lactams leads to substantially different modes of bulge formation. This is also consistent with the fact that glycopeptide antibiotics, which inhibit cell-wall synthesis nonspecifically, induce diverse modes of bulge formation (Huang et al., 2008).

The fact that we also observed variability in bulge formation across isogenic cells treated with the same drug suggests that cells vary in cellular states or components that affect the cell-wall damage caused by beta-lactams. We tested whether the rate of bulge formation depends on the cell-elongation state upon exposure to the drug. However, we found that initial cell length, a proxy for cell states, is not correlated with either bulge-formation time or bulge lifetime. This lack of correlation is probably because cephalaxin does not act until the localization of FtsI, a late event in the bacterial cell cycle (Goehring and Beckwith, 2005). This observation suggests that cell-cell variability in other components that affect PG biogenesis and metabolism (e.g., PG hydrolases) might underlie the observed heterogeneity in bulge formation across isogenic cells. The ability to quantitatively characterize bulge stability enabled by our imaging platform can be used as a tool to explore the contribution of such cellular components to cell lysis.

The metastability of the bulge and its dependence on the integrity of the OM suggest that an intact OM can support some level of turgor pressure. It is interesting to speculate that this mechanical strength of the OM may also play a role in counterbalancing turgor pressure in intact cells, adding to the mechanical support provided by the cell wall. It is worth noting two observations supporting this idea. First, Gram-positive bacteria, which lack the added support from the OM, are known to have a much thicker cell wall compared to their Gram-negative counterparts. Second, studies have shown that host-cell lysis by bacteriophage lambda requires the Rz-Rz1 complex, which disrupts the OM after cell-wall destruction (Berry et al., 2008). Taken together, these observations suggest a mechanical role for the OM in stabilizing the cell envelope in bulging cells and possibly also in intact cells under normal physiological conditions. Given that lysis requires failure of both PG and the OM, OM-targeting therapeutics combined with beta-lactam antibiotics might promote the antibiotics' efficacy and reduce the incidence of resistance. The recognition that the OM stabilizes bulging cells may therefore have important clinical implications.

EXPERIMENTAL PROCEDURES

Bacterial Strains, Plasmids, and Media

The wild-type strain used in this study is JOE309 (Chen and Beckwith, 2001), derived from *E. coli* K-12 strain MC4100. The *lptD* mutant (MC4100 *.lptD::kan* pET23/42 *lptD* .529–538) and the fluorescent strain with an OM marker (TB28(attHK MM47) Plac::ssPal-mCherry) are described in our recent work (Freinkman et al., 2011) and work from the Bernhardt lab (Paradis-Bleau et al., 2010). The fluorescent strain with an IM marker (ZipA-mCherry) was kindly provided by the Bernhardt lab. All live-cell time-lapse experiments were performed in Miller's LB (Luria broth) agarose pads at 37°C. Beta-lactam antibiotics were all freshly prepared and added into melted LB agarose before each experiment. All cells were treated with 50 µg/mL cephalixin, unless noted otherwise.

Fluorescence Microscopy

Cells were taken from an overnight culture, diluted by 100-fold, and allowed for further growth in LB for 2 hr at 37°C to reach early exponential phase (optical density [OD_{600nm}] = ~0.05). After that, beta-lactam antibiotics were added into the liquid culture and cells were grown in the presence of antibiotic treatment for ~30–90 min before imaging. Cells were sampled periodically throughout the treatment for examination of their morphology. For membrane staining, FM4-64 dye was added at the appropriate concentration. Cells were transferred from liquid culture onto drug-free LB agarose pads for imaging. Fluorescence images were taken immediately with appropriate filter sets for visualization of YFP, FM 46-4, and mCherry.

Live-Cell Time-Lapse Microscopy

Cells were first grown as described above into early exponential phase (OD_{600nm} = ~0.05). After that, cells were concentrated (10-fold) via centrifuge and resuspension. One microliter of the concentrated cell culture was then transferred onto a drug-containing LB agarose pad (200 µl) for live-cell microscopy with a 100× oil immersion objective. For spheroplast formation, 100 mM Mg²⁺ was also added into these LB agarose pads. All LB agarose pads were discs with a diameter of 1 cm and a height of 0.5 cm. The pads were also surrounded by a polydimethylsiloxane mold for creating an air pocket and were sealed by a cover glass for preventing evaporation. The final cell density on agarose pads was ~10⁶ cells/ml. Phase-contrast images were collected from the same field of view (containing ~25 cells) with auto focus on. All live-cell microscopy was performed using NIS-Elements software for control of a digital-imaging system coupled to an inverted microscope (model TE2000-E; Nikon). Image acquisition was carried out at 1 min/frame for the first

30 min after adding the drug and ~125 ms/frame after that, until final lysis (~2 hr after addition of the drug).

Single-Cell Movies with Adaptive Time Resolutions

In order to analyze the morphological dynamics of individual cells at adaptive time resolutions in accordance with processes that have different kinetics, we reduced the complete data set of ~30,000 frames of full field of view (~25 cells) to ~500 frames for each individual cell by applying a variable-sampling algorithm. The following two steps were implemented for generating these single-cell movies: (1) crop the regions containing individual cells within the full field of view and generate separate movies containing each single cell, and (2) apply varying time resolutions to four different phases of beta-lactam killing. One out of every 100 images was sampled for filamentation leading to bulge formation, and one out of every ten for bulge stagnation. For bulge formation and the lysis process, every image was selected for further analysis. This second step produced ~500 selected frames of single-cell images and established adaptive time resolutions. All image analysis, including computational analysis of single-cell shape dynamics, was implemented in MATLAB (MathWorks).

Image Analysis of Single-Cell Morphological Dynamics

The overall strategy of image analysis takes advantage of the dramatic change in pixel intensity across the cell boundary of the phase-contrast images (Guberman et al., 2008; Reshes et al., 2008). Four steps were implemented to characterize morphological features of single cells throughout beta-lactam treatment. First, cell area (number of pixels within the cell contour) was plotted against a wide range of threshold values. The plot showed a plateau region, where changing threshold values produces little cell-area change. The yellow cell contour was generated based on the medium value of this plateau range. Second, cyan and red lines were drawn manually for each single-cell movie for measuring bulge depth and cell length, respectively. Two intersection points between those lines and the cell contour were generated, and the distance between the two intersection points yielded the value of bulge depth and cell length for each frame. Third, bulge depth was plotted against time, and t_2 , t_3 , and t_4 were marked based on bulge-depth measurement for calculating bulge-formation time and bulge lifetime. Fourth, for the cracking angle, two angle lines were drawn on both sides of the cyan line for bulge depth. The intersection points of two angle lines and the line for bulge depth were used to calculate the cracking angle around the bulging region.

Recovery of the Bulging Cells

Cells were first grown as described above into early exponential phase (OD_{600nm} = ~0.05). After that, beta-lactam antibiotics and 100 mM Mg²⁺ was added into the liquid culture. Cells were then grown until OD_{600nm} reached a plateau (OD_{600nm} = ~0.2), harvested immediately, and washed twice with LB supplemented with 100 mM Mg²⁺ before transfer onto drug-free LB agarose pads for live-cell microscopy. Agarose pads were also supplemented with 100 mM Mg²⁺ to prevent premature cell lysis.

SUPPLEMENTAL INFORMATION

Supplemental Information includes five figures, five movies, and Supplemental Experimental Procedures and can be found with this article online at <http://dx.doi.org/10.1016/j.molcel.2012.09.016>.

ACKNOWLEDGMENTS

We thank Timothy Mitchison and Michael Springer for discussions and advice, and Thomas Bernhardt, Michael Elowitz, Elizaveta Freinkman, Adam Palmer, Thomas Silhavy, and Natividad Ruiz for comments on the manuscript. This work was supported by National Institutes of Health grant 5R01GM081617-05 (to R.K.) and National Institute of Allergy and Infectious Diseases grant AI081059 (to D.K.).

Received: January 2, 2012

Revised: June 13, 2012

Accepted: September 10, 2012

Published online: October 25, 2012

REFERENCES

- Berry, J., Summer, E.J., Struck, D.K., and Young, R. (2008). The final step in the phage infection cycle: the Rz and Rz1 lysis proteins link the inner and outer membranes. *Mol. Microbiol.* **70**, 341–351.
- Birdsell, D.C., and Cota-Robles, E.H. (1967). Production and ultrastructure of lysozyme and ethylenediaminetetraacetate-lysozyme spheroplasts of *Escherichia coli*. *J. Bacteriol.* **93**, 427–437.
- Chen, J.C., and Beckwith, J. (2001). FtsQ, FtsL and FtsI require FtsK, but not FtsN, for co-localization with FtsZ during *Escherichia coli* cell division. *Mol. Microbiol.* **42**, 395–413.
- Chung, H.S., Yao, Z., Goehring, N.W., Kishony, R., Beckwith, J., and Kahne, D. (2009). Rapid beta-lactam-induced lysis requires successful assembly of the cell division machinery. *Proc. Natl. Acad. Sci. USA* **106**, 21872–21877.
- Daly, K.E., Huang, K.C., Wingreen, N.S., and Mukhopadhyay, R. (2011). Mechanics of membrane bulging during cell-wall disruption in gram-negative bacteria. *Phys. Rev. E Stat. Nonlin. Soft Matter Phys.* **83**, 041922.
- de Pedro, M.A., Hötjje, J.V., and Schwarz, H. (2002). Fast lysis of *Escherichia coli* filament cells requires differentiation of potential division sites. *Microbiology* **148**, 79–86.
- Freinkman, E., Chng, S.S., and Kahne, D. (2011). The complex that inserts lipopolysaccharide into the bacterial outer membrane forms a two-protein plug-and-barrel. *Proc. Natl. Acad. Sci. USA* **108**, 2486–2491.
- Funahara, Y., and Nikaido, H. (1980). Asymmetric localization of lipopolysaccharides on the outer membrane of *Salmonella typhimurium*. *J. Bacteriol.* **141**, 1463–1465.
- Gerding, M.A., Ogata, Y., Pecora, N.D., Niki, H., and de Boer, P.A. (2007). The trans-envelope Tol-Pal complex is part of the cell division machinery and required for proper outer-membrane invagination during cell constriction in *E. coli*. *Mol. Microbiol.* **63**, 1008–1025.
- Goehring, N.W., and Beckwith, J. (2005). Diverse paths to midcell: assembly of the bacterial cell division machinery. *Curr. Biol.* **15**, R514–R526.
- Guberman, J.M., Fay, A., Dworkin, J., Wingreen, N.S., and Gitai, Z. (2008). PSICIC: noise and asymmetry in bacterial division revealed by computational image analysis at sub-pixel resolution. *PLoS Comput. Biol.* **4**, e1000233.
- Hamad, B. (2010). The antibiotics market. *Nat. Rev. Drug Discov.* **9**, 675–676.
- Hötjje, J.V. (1998). Growth of the stress-bearing and shape-maintaining murein sacculus of *Escherichia coli*. *Microbiol. Mol. Biol. Rev.* **62**, 181–203.
- Huang, K.C., Mukhopadhyay, R., Wen, B., Gitai, Z., and Wingreen, N.S. (2008). Cell shape and cell-wall organization in Gram-negative bacteria. *Proc. Natl. Acad. Sci. USA* **105**, 19282–19287.
- Jacoby, G.H., and Young, K.D. (1991). Cell cycle-independent lysis of *Escherichia coli* by cefsulodin, an inhibitor of penicillin-binding proteins 1a and 1b. *J. Bacteriol.* **173**, 1–5.
- Joseleau-Petit, D., Liébart, J.C., Ayala, J.A., and D'Ari, R. (2007). Unstable *Escherichia coli* L forms revisited: growth requires peptidoglycan synthesis. *J. Bacteriol.* **189**, 6512–6520.
- Kamio, Y., and Nikaido, H. (1976). Outer membrane of *Salmonella typhimurium*: accessibility of phospholipid head groups to phospholipase c and cyanogen bromide activated dextran in the external medium. *Biochemistry* **15**, 2561–2570.
- Lederberg, J., and St Clair, J. (1958). Protoplasts and L-type growth of *Escherichia coli*. *J. Bacteriol.* **75**, 143–160.
- Nikaido, H., and Vaara, M. (1985). Molecular basis of bacterial outer membrane permeability. *Microbiol. Rev.* **49**, 1–32.
- Pagès, J.M., James, C.E., and Winterhalter, M. (2008). The porin and the permeating antibiotic: a selective diffusion barrier in Gram-negative bacteria. *Nat. Rev. Microbiol.* **6**, 893–903.
- Paradis-Bleau, C., Markovski, M., Uehara, T., Lupoli, T.J., Walker, S., Kahne, D.E., and Bernhardt, T.G. (2010). Lipoprotein cofactors located in the outer membrane activate bacterial cell wall polymerases. *Cell* **143**, 1110–1120.
- Reshes, G., Vanounou, S., Fishov, I., and Feingold, M. (2008). Cell shape dynamics in *Escherichia coli*. *Biophys. J.* **94**, 251–264.
- Silhavy, T.J., Kahne, D., and Walker, S. (2010). The bacterial cell envelope. *Cold Spring Harb. Perspect. Biol.* **2**, a000414.
- Spratt, B.G. (1975). Distinct penicillin binding proteins involved in the division, elongation, and shape of *Escherichia coli* K12. *Proc. Natl. Acad. Sci. USA* **72**, 2999–3003.
- Tipper, D.J., and Strominger, J.L. (1965). Mechanism of action of penicillins: a proposal based on their structural similarity to acyl-D-alanyl-D-alanine. *Proc. Natl. Acad. Sci. USA* **54**, 1133–1141.
- Typas, A., Banzhaf, M., van den Berg van Saparoea, B., Verheul, J., Biboy, J., Nichols, R.J., Zietek, M., Beilharz, K., Kannenberg, K., von Rechenberg, M., et al. (2010). Regulation of peptidoglycan synthesis by outer-membrane proteins. *Cell* **143**, 1097–1109.
- Wise, E.M., Jr., and Park, J.T. (1965). Penicillin: its basic site of action as an inhibitor of a peptide cross-linking reaction in cell wall mucopeptide synthesis. *Proc. Natl. Acad. Sci. USA* **54**, 75–81.